

Light-particle emission from the fissioning nuclei ^{126}Ba , ^{188}Pt and $^{266,272,278}\text{110}$: theoretical predictions and experimental results *

K. Pomorski^a, B. Nerlo-Pomorska^a, A. Surowiec^a, M. Kowal^a,
J. Bartel^b, K. Dietrich^c, J. Richert^d, C. Schmitt^b,
B. Benoit^{b,e}, E. de Goes Brennand^{e†}, L. Donadille^f, C. Badimon^g
^a*Katedra Fizyki Teoretycznej, Uniwersytet Marii Curie-Skłodowskiej,
Lublin, Poland*
^b*Institut de Recherches Subatomiques, Strasbourg, France*
^c*Physik Department, Technische Universität München, Germany*
^d*Laboratoire de Physique Théorique, Université Louis Pasteur,
Strasbourg, France*
^e*Université Libre de Bruxelles, Belgium*
^f*University of Birmingham, United Kingdom*
^g*Centre d'Etudes Nucléaires de Bordeaux-Gradignan, France*

Abstract

We present a comparison of our model treating fission dynamics in conjunction with light-particle (n, p, α) evaporation with the available experimental data for the nuclei ^{126}Ba , ^{188}Pt and three isotopes of the element $Z=110$. The dynamics of the symmetric fission process is described through the solution of a classical Langevin equation for a single collective variable characterizing the nuclear deformation along the fission path. A microscopic approach is used to evaluate the emission rates for pre-fission light particles. Entrance-channel effects are taken into account by generating an initial spin distribution of the compound nucleus formed by the fusion of two deformed nuclei with different relative orientations.

PACS number: 24.75.+i, 25.85.-w, 25.60.Pj, 25.70-z

Keywords: fission dynamics, light particle emission, entrance channel effects.

*The work is partly supported by the Polish Committee of Scientific Research under Contract No. 2P03B 011 12

†On leave from Universidade Estadual da Paraíba, Brasil

1 Introduction

The dynamical time evolution of the fission process from an initially formed compound nucleus with a more or less compact shape to the saddle and scission configurations and the simultaneous emission during this deformation process of light particles constitutes a very complex problem. It is the aim of our study to describe this process taking into account the excitation of both thermal and rotational nature, the initial configuration and to calculate the evaporation of light particles from an excited, rotating, deformed nucleus on its way from the initial compact shape to the scission point.

In the absence of a complete microscopic ab initio theory of such a dynamical process, many different theoretical approaches aiming at its description have been worked out [6]-[9]. They generally rely on a classical description of the evolution of the collective coordinates which are introduced as abundant variables. In these descriptions, collective parameters appear (collective mass, friction, and diffusion coefficients) which depend on the collective coordinates. It seems clear that the quality of the theoretical description will depend on the more or less pertinent choice of the collective coordinates and the degree of realism of the underlying theory used to determine the collective parameter functions. The importance of pure quantum effects such as pairing correlations and the existence of shell effects which are present at low excitation energies has been investigated recently [10]-[14].

The multiplicity and the characteristics (energies, angular distributions, correlation functions) of prefission light particles and gamma emission may provide some useful information on the time evolution of the nucleus as it evolves towards the saddle and scission point. Observables like prefission light-particle multiplicities may, indeed, work as a clock. Angular distributions and particle correlations may give informations on the surface and deformation of the fissioning nucleus.

We recently developed a realistic time dependent model which described the time evolution of an excited nucleus as it is e.g. generated in a heavy-ion collision and decaying through symmetric fission with pre- and post-fission light particle emission [15]. We applied our description to the case of ^{160}Yb and made a detailed analysis of different physical quantities characterizing the decaying system. We found a rather good agreement of our theoretical predictions with the experimentally observed light-particle multiplicities.

More recently, several new sets of experimental data have become available [16]-[21] with a more complete analysis of the emitted light particles. It is the aim of the present work to systematically test our approach by a comparison with these experimental data. The fact that these data are obtained in quite different regions of the periodic table makes a comparison between calculated and experimental results all the more challenging.

A particular motivation for this work is the explicit description of the entrance channel through which the initial spin distribution of the system is generated. This is achieved by considering all possible relative orientations of the two colliding deformed nuclei in the entrance channel. Their different orientations and the different possible impact parameters of the reaction yield the initial spin distribution $d\sigma/dL$ versus L which determines the relative weights of the initial angular momentum of the compound nucleus with which the Langevin trajectories are started.

Still another motivation for the present work is the presentation of the link between the well known Weisskopf formula [22] and a new and more microscopically founded description of the emission width for the light particles in terms of phase-space densities of the particle to be emitted [23].

The paper is organized as follows: The dynamical model describing the time evolution of a deformed, hot, and rotating nucleus from its initial to a final configuration is presented in section 2. In section 3 we specify how to determine the emission rates for light particles from a hot, deformed and rotating nucleus moving along the previously described trajectory. In section 4 we show how we obtain the initial spin distribution which has been not considered in our previous study [15]. Our results concerning the nuclear systems ^{126}Ba , ^{188}Pt and $^{266,272,278}\text{110}$ are presented in section 5. The paper is closed in section 6 with a summary of the most relevant results and an outlook on planned extensions of the model.

2 Collective dynamics of an excited system

We consider an ensemble of deformed nuclei with finite excitation energies and rotational angular momenta as given by the initial conditions determined from the entrance channel. The subsequent time evolution of the nucleus is governed in our present description by a single collective coordinate $q = R_{12}/R_0$ where R_{12} is the distance between the two centers of mass of the left-right symmetric deformed nucleus and R_0 is the radius of the corresponding spherical nucleus having the same volume. This collective variable is defined in the framework of a Trentalange–Koonin–Sierk (TKS) [24] parameterization of the surface of the nucleus. The TKS deformation parameters are related to q by means of a minimization procedure of the collective potential energy defined below [25].

Denoting the conjugate momentum by $p(t)$ we use the following classical equations of motion to describe the time evolution of the fissioning nucleus [15]

$$\frac{dq}{dt} = \frac{p}{M(q)} \quad (1)$$

$$\frac{dp}{dt} = \frac{1}{2} \left(\frac{p}{M(q)} \right)^2 \frac{dM(q)}{dq} - \frac{dV(q)}{dq} - \frac{\gamma(q)}{M(q)} p + F_L(t). \quad (2)$$

Here $M(q)$ is the collective mass determined in the incompressible fluid approximation [26] and $\gamma(q)$ the friction coefficient calculated in the wall-and-window friction model [27]. The collective potential $V(q)$ is obtained as the difference of the Helmholtz free energy at deformation q minus the one for the ground-state deformation.

The free energy could in principle be obtained from a microscopic mean-field calculation at finite temperature. To perform such a constraint Hartree-Fock calculation using a reasonable effective nucleon-nucleon interaction of the Skyrme or Gogny type at every point in the multi-dimensional deformation space is, of course, completely out of question due to the tremendous computer time such an analysis would involve. Even to perform the same kind of calculation on the level of a selfconsistent semiclassical approximation like the Extended Thomas-Fermi (ETF) method [28] at finite temperature [29], which would describe the average nuclear structure without shell oscillations, would be far too time consuming. This is why we have rather used a still simpler semiclassical approach and the liquid drop model with the parametrization of Myers and Swiatecki [30] as explained in Appendix A. We have tested the barrier heights obtained in this way versus the ones obtained from selfconsistent semiclassical calculations (at zero temperature) and obtained agreement within a few MeV as described in Ref.[25]. These calculations describe, of course, deformation properties of non excited nuclei. In order to take

nuclear excitation into account we have used the temperature dependence of the LDM parameters associated with the Skyrme SkM* interaction [31], determined for that interaction through selfconsistent semiclassical calculations at finite temperature in Ref. [25].

To use the temperature dependence of the LDM parameters associated with the Skyrme SkM* force together with the Myers-Swiatecki parametrization of the LDM is, of course, inconsistent. Since approaches give very similar results for the semiclassical energy at zero temperature this approximation seems, however, very reasonable. The semiclassical approach used here is of course only an approximation at low temperatures since shell effects are absent from our description. It is however well known that nuclear shell effects are washed out with increasing nuclear temperature and have essentially disappeared beyond $T \simeq 2.5\text{-}3$ MeV. At these temperatures the semiclassical results are becoming exact. For the cold systems the fission barriers obtained with this potential are higher than those evaluated by Sierk [33], but already at excitation energies $E^* \approx 90$ MeV both barriers become comparable and for $E^* > 90$ MeV the barriers evaluated in our model are even smaller than the Yukawa folded ones of Sierk.

The friction term and the Langevin force $F_L(t)$ in Eq. (2) generate the irreversible production of heat energy and the energy fluctuations respectively which both originate from the coupling of the collective dynamics to the intrinsic degrees of freedom. In practice one defines $F_L(t) = \sqrt{D(q)}f_L(t)$, where $D(q)$ is the diffusion coefficient. We take the simplifying point of view that it is related to the friction coefficient $\gamma(q)$ through the Einstein relation $D(q) = \gamma(q)T$, where T is the temperature of the system. The quantity $f_L(\tau)$ can be written in the form $f_L(\tau) = \sqrt{\tau}\eta$, where τ is a time step length corresponding to a time interval $[t, t+\tau]$ and η is a gaussian distributed random number with zero average $\langle \eta \rangle = 0$ and variance $\langle \eta^2 \rangle = 2$ where brackets represent ensemble averages.

The Einstein relation is in principle valid at high temperature, in a regime where the process can be described in a classical framework. Quantum effects (pairing, shell corrections, collective shape vibrations) may be present at low temperatures and modify the relation between D and γ [11]-[14]. We shall come back to this point later on.

In principle, one would have to treat each ensemble of nuclei with a given initial angular momentum L and a given initial excitation energy microcanonically. We assume that we may replace this microcanonical ensemble by a grand canonical one in which, instead of the mean excitation energy, the temperature T has a well-defined value at a given time. This simplifying assumption is innocuous as far as the mean values of observables are concerned, but it may falsify the fluctuations to a certain extent. We assume that the time scale which governs the fission dynamics is much larger than the internal equilibration time, otherwise the definition of a nuclear temperature would make no sense. Under these conditions the system can be considered as being continuously close to equilibrium. We suppose that the nuclear excitation energy E^* is related to T through the usual Fermi-gas expressions $E^* = a(q)T^2$, where $a(q)$ is the level density parameter at a given deformation q .

For practical calculations Eqs. (1) and (2) are rewritten in a discretized form and numerically integrated over small time steps τ [15]. In order to perform such an integration one needs to start from some fixed initial conditions which define the beginning of the process. We take into account the possible emission of light particles in every time step and we make sure that the average total energy of the system will be conserved. This determines the nuclear excitation energy and hence the temperature at each instant of time.

3 Particle emission from a hot, deformed, and rotating nucleus

Particle emission before scission is governed by transition rates $\Gamma_\nu^{\alpha\beta}(E^*, L)$ which determine the number of particles of type ν (we take into account neutrons, protons, and α particles) emitted per unit time with an energy e_α in an interval $[e_\alpha - \frac{1}{2}\Delta e, e_\alpha + \frac{1}{2}\Delta e]$ and with an angular momentum ℓ_β from a nucleus with average excitation energy E^* and total angular momentum L . In Ref. [15] we used the well known Weisskopf formula [22] for the partial width $\Gamma_\nu^{\alpha\beta}(E^*, L)$ in terms of densities of states of the emitting and residual nucleus and of the transmission coefficient $w_\nu(e, \ell_\beta)$ for emitted a particle ν with given energy e and angular momentum ℓ_β . The determination of w_ν takes into account the deformation and rotation of the emitting nucleus (see Appendix B of Ref. [15] for details).

In Ref. [23] another more microscopic determination of these transition rates was proposed. In this framework the transition rates $\Gamma_\nu^{\alpha\beta}$ are given as

$$\Gamma_\nu^{\alpha\beta} = \frac{d^2 n_\nu}{d\varepsilon_\alpha d\ell_\beta} \Delta\varepsilon \Delta\ell, \quad (3)$$

where ε_α and ℓ_β characterize an emission energy and angular momentum lying in the intervals

$$\left[\varepsilon_\alpha - \frac{1}{2}\Delta\varepsilon, \varepsilon_\alpha + \frac{1}{2}\Delta\varepsilon\right] \quad \text{and} \quad \left[\ell_\beta - \frac{1}{2}\Delta\ell, \ell_\beta + \frac{1}{2}\Delta\ell\right]$$

respectively.

The number n_ν of particles of type ν which are emitted per time unit through the surface Σ of the fissioning nucleus is given by [23]

$$n_\nu = \int_\Sigma d\sigma \int d^3p' f_\nu(\vec{r}'_0, \vec{p}') v'_\perp(\vec{r}'_0) w_\nu(v'_\perp(\vec{r}'_0)) \quad (4)$$

where \vec{p}' , \vec{v}' are the momentum and velocity in the body-fixed frame. The quantity v'_\perp is the velocity component perpendicular to the emission surface at the surface point \vec{r}'_0 . The $\vec{p}' = m\vec{v}' + m\vec{\omega} \times \vec{r}'$ is the momentum of the particle of mass m in the laboratory reference frame and $\vec{\omega}$ the angular velocity of the nucleus in this frame. Here and henceforward, primed quantities refer to the body-fixed frame.

The classical distribution in phase space reads

$$f_\nu(\vec{r}', \vec{p}') = \frac{2}{h^3} \frac{\theta(\vec{r}')}{1 + \exp\left[\frac{1}{T} \left(\frac{p'^2}{2m} + U - \omega\ell' - \mu_\nu\right)\right]}. \quad (5)$$

The θ function is 1 if \vec{r}' lies inside the nuclear volume or on its surface Σ and zero otherwise. The quantity μ_ν is the chemical potential and ℓ' the body-fixed angular momentum in the direction perpendicular to the axis of rotational symmetry of the deformed nucleus. The potential U is taken as

$$U(\vec{r}') = -V_0 + V_{Cb}(\vec{r}'), \quad (6)$$

where $V_0 > 0$ is chosen as a constant mean field potential and V_{Cb} is the Coulomb potential experienced at \vec{r}' by protons.

The quantity $w_\nu(v'_\perp(\vec{r}'_0))$ is the classical transmission coefficient for the emission of a particle of type ν . The transmission factor w_ν was chosen to be the one of an inverted harmonic oscillator [15].

The explicit relation of (3) with the Weisskopf formulation is discussed in Appendix B for a spherical emitting nucleus with angular momentum $L = 0$. The rates given by (3) can be worked out numerically if the distribution function in the phase space is known, what is the case for the neutrons and protons but not for the α -particles. We are working on a model which describes the distribution of α -particles by folding of the distributions of four ($2n$ and $2p$) correlated particles. The present approach is like the one of Ref. [15] and it allows us, in principle, to determine the particle emission in a given direction of space, hence the determination of observables like angular distributions and particle-particle correlation functions. Such observables may be worked out in the future. We did not attempt to do it here because of the lack of corresponding experimental data.

The transition rates $\Gamma_\nu^{\alpha\beta}$ are used in a simulation algorithm by means of which we determine at each time step $[t, t + \tau]$ along each classical trajectory whether a particle of given type with an energy and angular momentum in given intervals is emitted or not from the compound nucleus. Since the algorithm is already described in detail in Ref. [15] we do not repeat it here.

3.1 Initial conditions and energy balance

In order to integrate the classical equations (1) and (2) we need to fix the initial conditions from which the compound system starts and evolves either through a fission channel to its saddle and scission point or stays as a compound system which only emits light particles, i.e. ends up as an evaporation residue.

All the experimental systems which are considered in the next section are generated by means of heavy ion collisions at some bombarding energy. The nuclei which are involved in the reaction process can be deformed. The initial conditions corresponding to the origin of time are fixed by q_0 and p_0 , the initial value of the collective variable and its conjugate momentum and the spin distribution of the system which fixes the relative weight of the angular momentum of the initial compound systems.

The coordinate q_0 is fixed at the value of q where the collective potential $V(q)$ is minimal and its conjugate momentum is drawn from a normalized gaussian distribution

$$P(p_0) = (2\pi MT_0)^{1/2} \exp(-p_0^2/2MT_0), \quad (7)$$

where $M = M(q_0)$ is the collective mass. The initial temperature T_0 is obtained through $E_0^* = a(q_0)T_0^2$, where E_0^* is the initial excitation energy which can be obtained from the knowledge of the total energy as explained below.

In the reaction process, the compound nucleus can be formed with different values of the angular momentum. If both nuclei are spherical it is easy to construct the initial spin distribution under the assumption that the reaction cross section is given by the geometrical expression

$$\frac{d\sigma(L)}{dL} = \frac{\pi}{k^2}(2L + 1), \quad (8)$$

where k is the wavenumber of the relative motion.

The situation is more complicated if one or both initial nuclei are deformed. In principle one should then consider all possible relative orientations of the nuclei and follow their relative

trajectories from an infinite distance up to fusion. This implies the knowledge of the nuclear and Coulomb potential for given relative distance between the centers of mass and given orientation. This raises intricate problems which have been considered by several authors [34, 35, 36] but not yet solved in their full generality.

In a first step we want to avoid such cumbersome calculations and restrict ourselves to a simplified procedure which has been already proposed in former work [36, 37]. In practice we consider the scattering of spherical ions of fixed energy E and introduce the gaussian energy distribution with the width

$$\Delta E = \delta E + \Delta_1 E + \Delta_2 E, \quad (9)$$

where δE is the experimental beam width, $\Delta_1 E$ describes the slowing down of the projectile in the target, and the quantity $\Delta_2 E$ is the difference of the Coulomb barriers between two extreme geometries of touching spheroidally deformed nuclei, i.e. with aligned (tip on tip) or parallel (side on side) z -axes.

One can now work out the classical trajectories describing the relative motion of the equivalent spherical ions for every initial angular momentum L in $[0, L_{\max}]$, where L_{\max} is the maximal angular momentum for the colliding ions and for a sufficient number of energy values within the distribution defined above.

Repeating the trajectory calculations leads to the spin distribution

$$\left(\frac{d\sigma_F}{dL} \right)_{L_i} = \frac{2\pi}{k^2} L_i \frac{N_i^F}{N_i}, \quad (10)$$

where L_i is the considered angular momentum, N_i^F is the number of trajectories which lead to fusion and N_i is the total number of trajectories. The quantity k is the wave-number of the relative motion of the incident nuclei. The present procedure, even though it is not rigorous, leads to spin distributions which are rather realistic [36, 37].

Finally, in order to describe the evolution of the excited compound system one needs to follow the evolution of the average excitation energy along the trajectory. This is achieved by the requirement of energy conservation.

At the initial point of a trajectory the total available energy can be written as

$$\begin{aligned} E_{\text{tot}} &= E_{\text{coll}} + E_{\text{rot}} + E_0^* \\ &= \frac{p_0^2}{2M(q_0)} + V(q_0) + \frac{L_0^2}{2J(q_0)} + E_0^*. \end{aligned} \quad (11)$$

Here, $J(q_0)$ is the moment of inertia of the compound system taken as a rigid deformed rotator and E_0^* is the initial intrinsic excitation energy of the compound nucleus. The intrinsic excitation energy $E^*(t)$ at any given later time t can be determined from the energy balance

$$E_{\text{tot}} = E_{\text{coll}} + E_{\text{rot}} + E_0^* + B_\nu + e_\alpha + E_{\text{recoil}}, \quad (12)$$

where B_ν is the binding energy of the emitted particle, different from zero only for α -particles, e_α is the kinetic energy of the emitted particle and E_{recoil} is the recoil energy of the nucleus after the emission of a particle, which can be neglected in practical calculations.

For each choice of the initial conditions one generates a separate trajectory. Emitted particles are counted with their energy and angular momentum. If the system overcomes the fission barrier the trajectory (event) contributes to the final fission cross section

$$\sigma_{\text{fiss}} = \sum_i \frac{d\sigma_{\text{fiss}}}{dL_i} = \sum_i \left(\frac{d\sigma_F}{dL_i} \right)_{L_i} \cdot \frac{N_i^{\text{fiss}}}{N_i^F}, \quad (13)$$

where N_i^{fiss} is the number of trajectories which lead to fission, and N_i^F – the number of fused trajectories at a given angular momentum L_i . The sum runs over all angular momentum bins and $d\sigma_F/dL$ is the fusion cross section given by Eq. (10).

The numbers of prefission particles obtained for each angular momentum of the compound nucleus (M_ν) are weighed with the differential fission cross section in order to obtain the measured number of particles emitted in coincidence with fission:

$$\langle M_\nu \rangle = \frac{\sum_i \frac{d\sigma_{\text{fiss}}}{dL_i} \cdot M_\nu(L_i)}{\sigma_{\text{fiss}}} . \quad (14)$$

4 Application of the model to various experimentally studied systems

In the present section we aim to confront experimental results concerning the multiplicities of emitted particles in coincidence with symmetric fission events with the model described in the preceding section. All measured and calculated data are presented in Table 1 for three systems: ^{126}Ba , ^{188}Pt , and $^{266,272,278}110$ obtained by different entrance channels and at different energies. These data result from experiments performed at the SARA (Grenoble) and the VIVITRON (Strasbourg) [16]-[20] using the DEMON neutron detector [38, 39]. Unfortunately, the charged particles (p, α) were not measured, so we give in Table 1 the theoretical predictions only. We present a more detailed discussion of the results for each system in the next subsections.

4.1 The ^{126}Ba compound system

The compound nucleus ^{126}Ba has been experimentally produced through two different entrance channels:

(I) $^{28}\text{Si} + ^{98}\text{Mo} \rightarrow ^{126}\text{Ba}$ at $E_{\text{lab}}=204, 187, \text{ and } 166 \text{ MeV}$
and

(II) $^{19}\text{F} + ^{107}\text{Ag} \rightarrow ^{126}\text{Ba}$ at $E_{\text{lab}}=148 \text{ and } 128 \text{ MeV}$.

Fig. 1 shows the fusion cross-section and the fission yields as a function of the initial angular momentum. The distributions of the initial angular momentum were calculated with the help of the corresponding Langevin equation [5, 9, 36] for two different entrance channels (I, II) and various bombarding energies. As it can be seen, the fission yields are rather small and located in the tails of the distributions. This observation which also holds for many other systems implies that it is of great importance to calculate carefully the dependence of the fusion cross-section on the angular momentum if one wants to describe the competition between the decay of the compound nucleus by fission and by light particle emission in a correct way. Concerning Fig. 1 we also note that the dominant part of the initial excitation energy resides in the collective rotational motion. One observes in Fig. 1 a general increase of the fission cross section with the excitation energy of the compound nucleus ^{126}Ba with the only exception of the highest excitation energy. In that case the emission of α -particles becomes important and competes with the fission process. This causes a substantial loss of internal energy due to particle emission which in turn leads to an increase of the fission barrier and therefore to a smaller fission yield.

In Fig. 2, the potential energy V_{fiss} of the fissioning nucleus ^{126}Ba for different angular momenta is plotted as a function of the relative distance between fission fragments. One can

see in Fig. 2 that the fission barrier of the fused nucleus at temperature $T=1.6$ MeV and angular $L=0$ is quite high in our model. It is equal to 43 MeV. It vanishes at very large angular momentum ($L \approx 80\hbar$). The high temperature can also reduce significantly the fission barrier as one can learn from Fig. 3, where the free energy of ^{126}Ba is plotted for a few temperatures between 0 and 4.8 MeV. This is why one can observe a significant fission rate only at large angular momenta and high excitation energies. All curves representing the fission barriers in Figs. 2 and 3 end at the scission point region. It is seen from Figs. 2 and 3 that the saddle and scission points are close to each other for ^{126}Ba .

Part of the excitation energy of ^{126}Ba is contained in the rotational mode. In Fig. 4, the temperature of ^{126}Ba corresponding to different excitation energies is plotted as a function of angular momentum. One can see that, at the lowest excitation energy $E^*=84$ MeV and the highest angular momentum, the temperature is 0.5 MeV only. This means that our theoretical predictions based on the statistical equilibrium could be too rough in this case.

The experimental neutron multiplicities obtained for both the fission and the fusion channel are shown in Table 1 along with the calculated neutron, proton, and α -particle multiplicities.

In Figs. 5 and 6, we show the calculated average numbers of neutrons, protons, and α -particles emitted in coincidence with fission as a function of the excitation energy E^* of the initial compound nucleus. The initial compound nucleus ^{126}Ba is produced by the fusion reaction (I) in Fig. 5, and in Fig. 6 the same initial compound nucleus originates from the fusion reaction (II). Only the n -emission on the way to fission has been measured so far. The measured numbers of prefission neutrons are indicated by points with error bars. At two excitation energies we have measurements for the two different entrance channels. As one can read from Table 1 at the excitation energy $E^* = 101.4$ MeV the measured and calculated numbers of emitted prefission neutrons (in coincidence with fission) are $M_n = 1.32$ and 1.83, resp., for the entrance channel (I) (Fig. 5) and $M_n = 1.31$ and 1.80, resp., for the entrance channel II (Fig. 6). At the higher excitation energy $E^* = 118.5$ MeV the measured and calculated numbers of emitted neutrons are $M_n = 2.01$ and 1.71 for the entrance channel (I) (Fig. 5) and $M_n = 1.85$ and 1.99 for the entrance channel (II) (Fig. 6).

The experimentally observed number of emitted prefission neutrons at given excitation energy E^* of the initial compound nucleus is thus larger for the entrance channel (I) than for the entrance channel (II) and the difference of the number of emitted neutrons is seen to be larger for the larger excitation energy.

The interpretation of this observation is that for ^{126}Ba only the compound nuclei formed with high angular momentum may undergo fission and thus give rise to prefission neutrons because the fission barrier for low angular momentum is high (≥ 15 MeV). For $T=1.6$ MeV the LD fission barriers vanish for about $L = 70 \hbar$ as can be seen from Fig. 2. Thus the main part of the prefission neutrons is obtained for angular momenta around $L = 80 \hbar$ as indicated in Fig. 1. At given excitation energy E^* the number of compound nuclei formed with such high angular momentum is larger for the entrance channel (I) with ^{28}Si as a projectile than for the entrance channel (II) with ^{19}F as a projectile (see Fig. 1).

The theoretically estimated prefission proton multiplicities (M_p) are very small as one can see in Figs. 5 and 6. The multiplicities of α -particles are not negligible at the highest ($E^*=131.7$ MeV) and the lowest ($E^*=84.1$ MeV) excitation energies (see Figs. 5 and 6). The increase of M_α at high excitation energy is mostly due to the high temperature effects while the unexpectedly large number of emitted α -particles at $E^*=84.1$ MeV is mostly due to the large deformation of the emitter and the huge centrifugal potential ($L \geq 80\hbar$) reducing the already small Coulomb barrier for the α -particles at the tips even further.

As for the comparison of measured and calculated numbers of emitted prefission neutrons, the general agreement is not unsatisfactory. Nevertheless, one notices that the calculated average emission numbers are larger than the observed ones for the higher excitation energy $E^* = 118.5$ MeV. If, instead of the temperature-independent friction, which underlies these calculations, we would use a friction parameter increasing with temperature, the agreement might be better.

4.2 The ^{188}Pt compound system

As seen in Table 1, the compound nucleus ^{188}Pt was produced at two excitation energies $E^*=100$ MeV and 66.5 MeV using two different reactions [16]

- $^{34}\text{S} + ^{154}\text{Sm} \rightarrow ^{188}\text{Pt}$ at $E_{lab} = 203$ and 160 MeV ,
- $^{16}\text{O} + ^{172}\text{Yb} \rightarrow ^{188}\text{Pt}$ at $E_{lab} = 138$ MeV.

The theoretical estimates of the initial spin distributions (solid lines) as well as the fission rates (bars) for $E^*=100$ MeV and two entrance channels as well as for $E^*=66.5$ MeV are plotted in Fig. 7 as functions of angular momentum of the compound nucleus. It is seen that each reaction leads to different spin distribution. These differences are responsible for the entrance channel effects in the prefission neutron multiplicities emitted by ^{188}Pt at $E^*=100$ MeV (see Table 1).

Similarly, as in the case of ^{126}Ba , we present in Fig. 8 the fission barriers of ^{188}Pt obtained for different angular momenta (L) at fixed temperature $T=1.6$ MeV. It is seen that for $T = 1.6$ MeV and $L = 70\hbar$ the fission barrier becomes negligible. Also one can see in Fig. 9 that with increasing temperature the fission barrier decreases. At $T = 4.8$ MeV and $L = 30\hbar$, the fission barrier of ^{188}Pt is about four times lower than for $T = 0$ and $L = 30\hbar$. Contrary to the case of ^{126}Ba , where the saddle point is very close to the scission point, the path from the saddle point ($q = R_{12}/R_0 \approx 1.6$) to the scission point ($q \approx 2.2$) of ^{188}Pt is much longer and will take more time. This implies that the case of ^{188}Pt is better suited to study the influence of dynamical effects on the prefission light-particle multiplicities.

The prefission neutron multiplicities theoretically predicted for ^{188}Pt are too small (by ~ 1 unit on the average) in comparison with the experimental data [16]. Also the effect of the entrance channel is not fully reproduced. Unfortunately the protons and α -particle multiplicities were not measured, so we cannot test the predictive power of our model in this case.

4.3 The $Z = 110$, $N = 156, 162$, and 168 compound systems

Three isotopes of the superheavy compound nucleus with $Z = 110$ were formed by means of the following fusion reactions

- $^{58}\text{Ni} + ^{208}\text{Pb} \rightarrow ^{266}110$ [19]
- $^{64}\text{Ni} + ^{208}\text{Pb} \rightarrow ^{272}110$ [19]
- $^{40}\text{Ca} + ^{232}\text{Th} \rightarrow ^{272}110$ [20]
- $^{40}\text{Ar} + ^{238}\text{U} \rightarrow ^{278}110$ [20]

at different excitation energies between 66 MeV and 186 MeV. The prefission neutron multiplicities were determined experimentally and estimated theoretically within our model. Both the experimental and theoretical results are given in Table 1.

Using Langevin type equations to describe the fusion process [5, 9, 36] we obtained the initial spin distribution of compound nucleus. As an example, the differential fusion cross section is plotted in Fig. 10 for the reaction $^{40}\text{Ca} + ^{232}\text{Th}$ at $E_{\text{lab}}=250.4$ MeV as a function of the angular momentum of the system. The effective fission cross section is marked by bars in the figure. It is seen in Fig. 10 that only the lowest angular momenta contribute to the fusion fission process of $^{272}110$ due to the fact that the fission barrier of $^{272}110$ vanishes at $L > 22\hbar$. All isotopes of the element $Z=110$ have a rather small fission barrier which disappears rapidly with increasing spin (L). This is illustrated in Fig. 11, where the fission barriers of $^{266}110$ corresponding to a few L are plotted as functions of the elongation.

In our calculations we only took into account those trajectories for which the saddle point existed, i.e. we neglected the so-called quasifission events. The number of emitted prescission particles is mostly governed by the dynamics from the saddle to the scission point, but of course the initial conditions (see Section 3.1) play also an important role. In our model we used two different sets of Langevin equations. The first set of equations describes the fusion dynamics [5, 9] while the second one, coupled with the Master equations for particle emission, describes the fission process [15]. A better solution would be a model in which the whole dynamics from fusion to fission as well as the light particles emission would be described by one set of equations. Such an approach could immediately solve the problem of the proper setting of the initial conditions for the compound nucleus.

The experimental and theoretical prefission neutron multiplicities for $Z=110$ compound nuclei are written in Table 1 and additionally they are drawn in Fig. 12 as functions of the excitation energy of the system. The dashed lines correspond to the results obtained with the wall-and-window friction (γ_{ww}) reduced by 50% while the dotted lines stand for the results obtained with the standard value of γ_{ww} . It is seen that for the lowest excitation energies the agreement of theoretical results with the measurements of neutron multiplicities is good, while the discrepancy grows with increasing excitation energy. For the most excited compound nuclei our theoretical predictions are too large by 1 to 2 units. This result could mean that the effective time which the system needs to pass from the saddle to the scission point is too long in our model for a very hot compound nucleus. Any of transport coefficients do not depend on the temperature. This could be the reason of the observed discrepancy. In the near future we intend to perform a new calculation with temperature dependent transport coefficients evaluated within the linear response theory [13, 14]. The temperature dependence of the friction parameter could be important, because as one can see in Fig. 12 the reduction of the friction parameter by 50% decrease the neutron multiplicities by 1 to 0.5 units depending on the excitation energy of compound nucleus.

In our model the superheavy nucleus with $Z=110$ is already cold when it reaches the scission point after emission of some neutrons and α -particles. So the shell effects begin to play an important role for very deformed shapes. The shell effects could lead to the compact fission, i.e. splitting of the $Z=110$ nucleus into two spherical fragments. In our model the shell effects are not present but we simulate partially their influence on the number prefission particles by counting only those particles which have been evaporated before reaching the elongation of nucleus close to the compact scission point ($R_{12}/R_0 \sim 1.5$).

Contrary to the case of decay of ^{126}Ba and ^{188}Pt compound nuclei a hot superheavy nucleus with $Z=110$ exists and fissions at very low angular momenta ($L < 20\hbar$). This range of L corre-

sponds to the linear part of the differential fusion cross-section $d\sigma/dL$ (see Fig. 10), so we do not expect entrance channel effects on multiplicities of prefission neutrons.

The Coulomb barrier for emission of the charged particles from $Z=110$ isotopes is rather high so the predicted proton and α multiplicities are much smaller than the neutron multiplicities as one can see in Table 1.

5 Summary, conclusions and further developments

In the first part of the present work we described an extension of our model [15] used so far for describing the fission dynamics of an excited, rotating and possibly deformed compound system. We considered the decay of compound nuclei produced by the fusion of two heavy ions. The initial spin distribution was determined by a simple model calculation [5, 9] which took the possible deformation of the two ions into account [36]. Furthermore, we introduced the microscopic classical expression for the emission rates of light particles derived in reference [23] and showed the link of this expression with the Weisskopf formulation [22].

In the second part of the paper we presented a detailed comparison of the calculated neutron multiplicities with the ones obtained in different experiments involving systems from different regions of the mass table. All five systems discussed in the paper (^{126}Ba , ^{188}Pt and $Z=110$ isotopes) are good examples of different fission and particle evaporation mechanisms.

The light nucleus ^{126}Ba fissions at very high angular momenta ($L \sim 80\hbar$). Its saddle point is close to the scission point, so the fission dynamics plays a rather minor role in this case. The entrance channel effects influence significantly the decay properties of the excited ^{126}Ba , via different initial spin distributions of compound nucleus. Also huge centrifugal forces and big deformations corresponding to the saddle point lead in this case to a true competition between the neutron and α -particle evaporation. The experimental prefission neutron multiplicities grow with the excitation energy of ^{126}Ba while it is not always the case in our theoretical estimates.

In the case of ^{188}Pt the average angular momentum of the fissioning nucleus is around $60\hbar$, i.e. $20\hbar$ less than for ^{126}Ba . Also the way from the saddle point to the scission point is longer so that the dynamics from the saddle to the scission plays here an important role. In addition, the evaporation of a few particles does not increase so dramatically the height of the fission barrier as in the case for ^{126}Ba . As a consequence the fission process takes place during a longer time and the number of evaporated particles is larger. Similarly as in the case of ^{126}Ba the initial spin distribution (the entrance channel effect) influences the multiplicity of pre-fission neutrons which is here too small (by $\approx 30\%$) in comparison with the experimental data.

A completely different case is the decay of superheavy compound nuclei with $Z=110$. Here the way from the weakly deformed saddle point to the scission point is very long. The fission barrier of a hot compound nucleus with $Z=110$ is very small and it vanishes already at low angular momenta ($L < 22\hbar$). The way in which the $Z=110$ nuclei has been produced does not influence their decay properties since such nuclei exist at small angular momenta only, which belong to the linear part of the fusion cross-section $d\sigma/dL$. A majority of compound nuclei goes to fission with simultaneous emission of neutrons and α -particles. The number of prefission neutrons depends in this case on details of the fission dynamics, e.g. the slope of the potential and the magnitude of the friction and diffusion parameters. Our model overestimates slightly ($\approx 15\%$) the experimental number of prefission neutrons here. The neutron emission process cools significantly the $Z=110$ compound nuclei, so the temperature dependence of the friction and diffusion parameters could be “visible” in this case.

The present formulation of the model and its application can be improved on several points:

- (i) One may introduce a more detailed description of the formation process of the compound nuclei. Such a description will involve explicit trajectory calculations of the incident nuclei taking into account the nuclear and the Coulomb potentials for different relative initial orientations of the deformed nuclei. Calculations of relative potentials have been worked out in this framework [36, 37] but, to our knowledge, a full fledged dynamical trajectory calculation has yet to be done.
- (ii) The full treatment of fusion fission dynamics with simultaneous emission of the light particles will release us from a somewhat arbitrary choice of the initial conditions for the compound nucleus. Such a project is at present under investigation.
- (iii) We used a classical description of fluctuations and a form of the fluctuation-dissipation theorem which are valid for the case of high temperature. In fact, the temperature of the systems which we considered above could be low enough for quantum effects (pairing and shell effects) to play a non negligible role. This point has been investigated in the recent past [12, 13, 14] within the framework of nuclear transport theory [10]. It is our aim to come back to this point in the near future.
- (iv) Our fission barrier estimates need also further improvements. The present model bases on a modified (see Appendix A) liquid drop formula of Myers and Swiatecki [30] and it is known that for the cold light nuclei like ^{126}Ba it overestimates the fission barriers by ≈ 10 MeV [45].

For reasons of comparison with experiment we shall generalize our model taking asymmetric fission events into account. Many compound nuclei generated from mass asymmetric formation process channels appear with a high statistical weight.

Last but not least it would be nice to extend the test of the model to observables other than the light particle emission rates. Out-of plane particle angular distributions and correlations between emitted light particles would provide further sensitive tests of the validity of our approach. For instance, the ratio of neutrons emitted out of the reaction plane and within the reaction plane (defined by the beam and the outgoing fission fragments) would enable us to determine the deformation of the emitting compound nucleus.

Furthermore, we stress the importance of a measurement of the emitted neutrons, protons, and α -particles in the same system because the emission rates of these particles are reciprocally dependent on each other.

Acknowledgements

The authors J. B., K. D., and J. R. wish to express their thanks for the warm hospitality extended to them at the Institute for Theoretical Physics of the UMCS of Lublin.

References

- [1] W. Nörenberg, Phys. Lett. **B52** (1979) 289.
- [2] P. Grangé, H.C. Pauli and H.A. Weidenmüller, Phys. Lett. **B88** (1979) 9; Z. Phys. **A296** (1980) 107.
- [3] Y. Abe, C. Grégoire, H. Delagrange, J. Phys. **C4** (1986) 47.
- [4] Ch. Gregoire, H. Delagrange, K. Pomorski, K. Dietrich, Z. Phys. **A329** (1988) 497.
- [5] P. Fröbrich, J. Richert, Phys. Lett. **B237** (1990) 328.
- [6] E. Strumberger, W. Dietrich and K. Pomorski, Nucl. Phys. **A529** (1991) 522.
- [7] Y. Abe, S. Ayik, P.-G. Reinhard and E. Suraud, Phys. Rep. **275** (1996) 49.
- [8] P. Fröbrich, I.I. Gontchar, Phys. Rep. **292** (1998) 131.
- [9] W. Przystupa, K. Pomorski, Nucl. Phys. **A572** (1994) 153.
- [10] H. Hofmann, Phys. Rep. **284** (1997) 138.
- [11] S. Yamaji, H. Hofmann, R. Samhammer, Nucl. Phys. **A475** (1998) 487.
- [12] H. Hofmann, D. Kiderlen, Int. J. Mod. Phys. **E7** (1998) 243.
- [13] H. Hofmann, F.A. Ivanyuk, Phys. Rev. Lett. **82** (1999) 4603.
- [14] F.A. Ivanyuk, H. Hofmann, Nucl. Phys. **A657** (1999) 15.
- [15] K. Pomorski, J. Bartel, J. Richert and K. Dietrich, Nucl. Phys. **A605** (1996) 87.
- [16] C. Badimon, Ph. D. Thesis, Universite Bordeaux I, in progress and Nukleonika **43** (1998) 253.
- [17] B.Benoit, Ph.D.Thesis , Universite Libre de Bruxelles, Belgium, in progress.
- [18] E. de Goes Brennand, Ph. D. Thesis, Universite Libre de Bruxelles, Belgium, in progress and Nukleonika **43** (1998) 241.
- [19] L. Donadille et al., Nucl. Phys. **A656** 1999 256 and Ph.D. Thesis, Universite Paris'7 D. Diderot, France (1998), unpublished, and L. Donadille, B. Benoit et al., to be published.
- [20] B. Benoit, L. Donadille , I International Conference on the Chemistry and Physics of the Transactinide Elements, Seeheim, Germany, Sept. 26-30, 1999.
- [21] A. Kelic, et al., Europhys. Lett. **47** (1999) 552.
- [22] V. Weisskopf, Phys. Rev. **52** (1937) 295.
- [23] K. Dietrich, K. Pomorski and J. Richert, Z. Phys. **A351** (1995) 397.
- [24] S. Trentalange, S.E. Koonin and A.J. Sierk, Phys. Rev. **C22** (1980) 1159.

- [25] J. Bartel, K. Mahboub, J. Richert and K. Pomorski, Z. Phys. **A354** (1996) 59.
- [26] K.T.R. Davies, A.J. Sierk, J.R. Nix, Phys. Rev. **13C** (1976) 2385.
- [27] J. Blocki, J. Randrup and W. J. Swiatecki, Ann. Phys. **105** (1977) 427.
- [28] M. Brack, C. Guet and H.-B. Håkansson, Phys. Rep. **123** (1985) 275.
- [29] J. Bartel, M. Brack, M. Durand, Nucl. Phys. **A445** (1985) 263.
- [30] W.D. Myers, W.J. Swiatecki, Ark. Phys. **36** (1967) 343.
- [31] J. Bartel, P. Quentin, M. Brack, C. Guet, H.-B. Håkansson, Nucl. Phys. **A386** (1982) 79.
- [32] C. Guet, E. Strumberger, M. Brack, Phys. Lett. **205B** (1988) 427.
- [33] A.J. Sierk, Phys. Rev. **C33** (1986) 2039.
- [34] M. Arnould, W. M. Howard, Nucl. Phys. **A274** (1976) 295 and refs. therein.
- [35] N. Takigawa, T. Rumin, N. Ikara, LANL database nucl-th/9908071, August 24, 1999 and refs. therein
- [36] K. Pomorski, W. Przystupa and J. Richert, Acta Phys. Pol. **25B** (1994) 751.
- [37] K. Pomorski, W. Przystupa, J. Bartel and J. Richert, Acta Phys. Pol. **30B** (1999) 809.
- [38] M. Moszynski et al., Nucl. Instrum. Methods **A350** (1994) 226.
- [39] I. Tilquin et al., Nucl.Instrum. Methods **A365** (1995) 446.
- [40] P.B. Kahn, N. Rosenzweig, Phys. Rev. **187** (1970) 1193.
- [41] V.S. Ramamurthy, S.S. Kapoor, S.K. Kataria, Phys. Rev. **C5** (1972) 1124.
- [42] P. Möller, W.D. Myers, W.J. Swiatecki, J. Treiner, At. Data Nucl. Data Tables, **39** (1988) 225.
- [43] J. Blocki, J. Randrup, W.J. Swiatecki, C.W. Tsang, Ann. Phys. **105** (1977) 427.
- [44] J. Blocki, Y. Boneh, J.R. Nix, J. Randrup, M. Robel, A.J. Sierk and W.J. Swiatecki, Ann. Phys. **113** (1978) 330.
- [45] H.J. Krappe, J.R. Nix and A.J. Sierk, Phys. Rev. **C20** (1979) 992.

Appendix A: Transport parameters used in the Langevin equation

Fission dynamics correlated with prefission particle emission is generally described in a phenomenological framework, by means of quantities such as collective temperature-dependent potentials, masses, moments of inertia and friction coefficients.

The fission process is described here in terms of the unique collective variable $q = R_{12}/R_0$. The fission path parameterized by q is fixed by means of a minimalization of the free energy of a nucleus in the $(\alpha_0, \alpha_2, \alpha_4, \alpha_6)$ deformation space at a fixed temperature T . The deformation parameters are defined as follows [24]

$$\rho_s^2(z) = R_0^2 \sum_{\ell=0}^6 \alpha_{2\ell}(q) P_{2\ell}\left(\frac{z}{z_0}\right) , \quad -z_0 \leq z \leq z_0 , \quad (A1)$$

where the function $\rho_s(z)$ is the distance in cylindrical coordinates of any point of the surface to the symmetry axis.

The Helmholtz free energy of the nucleus plays the role of the collective potential and can be written, in a semiclassical approximation, as

$$F(N, Z, q, L, T) = E(N, Z, q, T=0) - a(N, Z, q) T^2 + E_{rot}(N, Z, q, L) . \quad (A2)$$

The first term on the r.h.s. of eq. (A2) is a liquid-drop (or any macroscopic model) type energy expressing the semiclassical energy of the deformed cold nuclear system as a function of the mass number $A = N + Z$, and the isospin asymmetry $I = (N - Z)/A$. The deformation dependence of the free energy is taken into account through the shape functions B_s and B_{coul} . The rotational energy is calculated explicitly as $E_{rot} = L^2/2\mathcal{J}(q)$ with a q -dependent rigid-body moment of inertia. We have used in eq. (A2) the liquid drop parametrization of Myers and Swiatecki [30].

The effects of excitation are taken into account in eq. (A2) through the level-density parameter a at a given deformation. As the Helmholtz free energy, which is the variational quantity, is given by

$$F(T) = E(T) - T S(T) \quad (A3)$$

with the temperature T as a Langrange multiplier, one can show [40, 41] that for a liquid-drop type system, entropy and excitation energy read

$$S = 2 a T \quad (A4)$$

and

$$E^* = E(T) - E(T=0) = a T^2 \quad (A5)$$

from which one obtains the last relation in eq. (A2).

The level density parameter a can be written in the form

$$a(N, Z, q) = a_v (1 + k_v I^2) A + a_s (1 + k_s I^2) A^{2/3} B_s(q) + a_{coul} Z^2 A^{-1/3} B_{coul}(q) , \quad (A6)$$

where the parameters $a_v=0.0533 \text{ MeV}^{-1}$, $k_v=0.5261$, $a_s=0.1059 \text{ MeV}^{-1}$, $k_s=2.7192$, and $a_{Coul}=0.000458 \text{ MeV}^{-1}$ are taken from Ref. [32]. In this expression, as well as in the macroscopic energy in eq. (A2), we have neglected the curvature and compression term proportional to $A^{1/3}$ since its coefficient for the cold system is known experimentally to be small [42]. When evaluating the Coulomb term in (A2) and (A6) the Coulomb exchange contribution is neglected.

To describe the fission dynamics one also needs to calculate the mass parameter $M(q)$ which enters the kinetic term of the equation of motion describing the fission process. In terms of the deformation parameter q the mass is given, in the incompressible fluid approximation [26], as

$$M = \pi \rho_0 \int_{-z_0}^{z_0} [\rho_s^2(z) A^2(z) + \frac{1}{2} B^2(z)] dz, \quad (A7)$$

where

$$A(z) = \frac{1}{\rho_s^2(z)} \frac{\partial}{\partial q} \int_z^{z_0} \rho_s^2(z') dz', \quad (A8)$$

and

$$B(z) = \frac{1}{2} \frac{\partial \rho_s^2}{\partial z} A + \frac{\partial \rho_s^2}{\partial q} \quad (A9)$$

and where $\rho_0 = 0.17 \text{ fm}^{-3}$ is the matter density.

The friction coefficient associated with the collective coordinate q is calculated in the framework of the wall and window model [43, 44]. The wall contribution, which is the dominant part of the friction parameter γ associated with the fission mode, is given by

$$\gamma = \frac{\pi}{2} \rho_0 \bar{v} \int_{-z_0}^{z_0} \frac{\left(\frac{\partial \rho_s^2}{\partial q} \right)^2}{\sqrt{\rho_s^2(z) + \frac{1}{4} \left(\frac{\partial \rho_s^2}{\partial z} \right)^2}} dz. \quad (A10)$$

where the average velocity \bar{v} of the nucleons inside the nucleus is at zero temperature defined as

$$\frac{\bar{v}}{c} = \frac{\bar{p}}{mc} = \frac{3}{4} \frac{\hbar}{mc} (3\pi^2 \rho_0)^{1/3} \quad (A11)$$

with the Fermi momentum $p_F = \hbar k_F = \hbar (3\pi^2 \rho_0)^{1/3}$.

Appendix B: Comparison between the microscopic semi-classical formulation of emission rates with the Weisskopf formula

In Ref. [23], a formulation of emission rates has been given which is based on the picture of a Fermi gas of nucleons at temperature T being confined to a deformed rotating square well. In this appendix we shall show that in the special case of a spherical well, the model of Ref. [23] becomes equivalent to Weisskopf's emission rate formula [22, 6]. We consider the example of neutron emission.

According to Ref. [23], the total number n of neutrons emitted per time unit is given by

$$n = \int_{\Sigma} d\sigma \int d^3p f_n(\vec{r}_0, \vec{p}) v_{\perp}(\vec{r}_0) w_0^{cl}(v_{\perp}(\vec{r}_0)), \quad (B1)$$

where $d\sigma$ is the infinitesimal element of the surface Σ at the surface point \vec{r}_0 . The momentum \vec{p} and the velocity \vec{v} of a neutron are related by the equation

$$\vec{p} = m\vec{v} + m\vec{\omega} \times \vec{r}, \quad (B2)$$

where \vec{r} is the position vector, m is the mass of the neutron, and $\vec{\omega}$ is the angular velocity of rotational motion of the nucleus. In the case of a spherical nucleus, a collective rotational motion is not possible. Consequently, we may put $\vec{\omega} = 0$ without loss of generality.

The Wigner function $f_n(\vec{r}_0, \vec{p})$ then describes a gas of fermions confined to a spherical well of depth V_0 at a temperature T . It is given by the expression

$$f_n(\vec{r}, \vec{p}) = \frac{2}{h^3} \cdot \frac{\theta(\vec{r})}{1 + \exp\left[\frac{1}{T} \left(\frac{p^2}{2m} - V_0 - \mu_n\right)\right]}, \quad (B3)$$

where $\theta(\vec{r})$ is a step function defined to be 1 for position vectors \vec{r} of points inside the volume Ω enclosed by the surface Σ

$$\theta(\vec{r}) = \begin{cases} 1 & \text{for } \vec{r} \in \Omega \text{ including } \Sigma \\ 0 & \text{otherwise} \end{cases}. \quad (B4)$$

The parameter μ_n is the chemical potential of the neutrons.

The last factor w_0^{cl} in formula (B1) is the semi-classical transmission coefficient for a neutron hitting the surface Σ at the point \vec{r}_0 with a velocity $v_{\perp}(\vec{r}_0)$ perpendicular to the surface. For a spherical surface Σ the unit vector normal to the surface at the surface point \vec{r}_0 is given by the radial unit vector

$$\vec{n}_{\Sigma}(\vec{r}_0) = \frac{\vec{r}_0}{R_0}, \quad (B5)$$

where $R_0 := |\vec{r}_0|$ is the radius of the square well potential.

In Weisskopf's theory of evaporation, the total number of emitted particles of a given sort is represented as an integral over the energy ε of the emitted particles [22, 6]. Consequently, we would like to rewrite the formula (B1) as an integral over the variable

$$\varepsilon = \frac{p^2}{2m} - V_0 \quad (B6)$$

performing at the same time the remaining integrations in a closed form. For this purpose let us first introduce polar coordinates (p, θ_p, φ_p) in momentum space choosing the surface unit vector $\vec{n}_\Sigma(\vec{r}_0)$ as the polar axis

$$\begin{aligned} p_\xi &= p \sin \theta_p \cos \varphi_p, \\ p_\eta &= p \sin \theta_p \sin \varphi_p, \\ p_\zeta &= p \cos \theta_p. \end{aligned}$$

In these coordinates the perpendicular velocity $v_\perp(\vec{r}_0)$ is given by

$$v_\perp(\vec{r}_0) = \frac{p \cos \theta_p}{m}. \quad (B7)$$

The transmission coefficient w_0^{cl} can only be unequal to zero, if the velocity $v_\perp(\vec{r}_0)$ is positive. Thus the polar angle θ_p can be restricted to the interval $0 \leq \theta_p \leq \pi/2$. The total neutron yield per time unit is thus given by

$$n = \frac{4\pi}{h^3} \int_\Sigma d\sigma \int_0^\infty dp \int_0^{\frac{\pi}{2}} d\theta_p \cdot \frac{p^3 \cos \theta_p \sin \theta_p}{m} w_0^{cl} \left(\frac{p \cos \theta_p}{m} \right) \cdot \left[e^{\frac{1}{T} \left(\frac{p^2}{2m} - V_0 - \mu_n \right)} + 1 \right]^{-1}. \quad (B8)$$

The surface integral yields for factor $4\pi R_0^2$. Instead of integration variables p and θ_p , we introduce the energy ε and the orbital angular momentum l of the neutron impinging on the surface

$$\varepsilon = \frac{p^2}{2m} - V_0, \quad (B9)$$

$$l = R_0 p \sin \theta_p. \quad (B10)$$

The Jacobian D of the transformation

$$D = \begin{vmatrix} \frac{\partial p}{\partial \varepsilon} & \frac{\partial \theta_p}{\partial \varepsilon} \\ \frac{\partial p}{\partial l} & \frac{\partial \theta_p}{\partial l} \end{vmatrix} \quad (B11)$$

is obtained from the inverse transformation

$$\begin{cases} p = \sqrt{2m(\varepsilon + V_0)} \\ \theta_p = \arcsin \left(\frac{l}{R_0 p} \right) = \arcsin \left(\frac{l}{R_0 \sqrt{2m(\varepsilon + V_0)}} \right) \end{cases} \quad (B12)$$

in the form

$$D = \frac{\sqrt{2m/(\varepsilon + V_0)}}{2\sqrt{2mR_0^2(\varepsilon + V_0) - l^2}}. \quad (B13)$$

In formulating the integration limits for the new variables ε and l we must take into account the condition

$$\frac{l^2}{2mR_0^2} \leq \frac{p^2}{2m} = \varepsilon + V_0, \quad (B14)$$

which implies that the total kinetic energy of the neutron can not be smaller than its rotational part.

The factor $p^3 \cos \theta_p \sin \theta_p$ can be written in terms of the new variables as follows

$$p^3 \cos \theta_p \sin \theta_p = 2m(\varepsilon + V_0) \sqrt{1 - \frac{l^2}{2mR_0^2(\varepsilon + V_0)}} \cdot \frac{l}{R_0}. \quad (B15)$$

Making use the Eqs. (B13) to (B15) we obtain for the r.h.s. of Eq. (B8):

$$\begin{aligned} n = & 2\pi \cdot \frac{2}{h^3} 4\pi R_0^2 \int_{-V_0}^{\infty} d\varepsilon \int_0^{\sqrt{2mR_0^2(\varepsilon+V_0)}} dl \frac{1}{2} \sqrt{\frac{2m}{(\varepsilon+V_0)}} \cdot \\ & \cdot \frac{2(\varepsilon+V_0)}{\sqrt{2mR_0^2(\varepsilon+V_0)-l^2}} \cdot \sqrt{1 - \frac{l^2}{2mR_0^2(\varepsilon+V_0)}} \cdot \frac{l}{R_0} \cdot \frac{w_0^{cl}(\varepsilon, l)}{[e^{(\varepsilon-\mu_n)/T} + 1]}, \end{aligned} \quad (B16)$$

or

$$n = \frac{(4\pi)^2}{h^3} \int_{-V_0}^{\infty} d\varepsilon \cdot \int_0^{\sqrt{2mR_0^2(\varepsilon+V_0)}} dl \cdot l \cdot \frac{w_0^{cl}(\varepsilon, l)}{[e^{(\varepsilon-\mu_n)/T} + 1]}. \quad (B17)$$

In Eq. (B17), the transmission coefficient $w_0^{cl}(\varepsilon, l)$ is obtained from $w_0^{cl}(v_{\perp})$ by expressing the argument v_{\perp} by the variables ε and l .

$$v_{\perp}(\varepsilon, l) = \frac{\sqrt{2mR_0^2(\varepsilon + V_0) - l^2}}{mR_0}. \quad (B18)$$

Introducing the dimensionless angular momentum λ instead of the variable l

$$l = \hbar \lambda, \quad (B19)$$

the formula (B17) takes the form

$$n = \int_{-V_0}^{\infty} d\varepsilon \int_0^{\lambda_{\max}(\varepsilon)} d\lambda \frac{\partial^2 n}{\partial \varepsilon \partial \lambda}, \quad (B20)$$

with

$$\frac{\partial^2 n}{\partial \varepsilon \partial \lambda} = \frac{4}{h} \frac{\lambda \cdot w^{cl}(\varepsilon, \lambda)}{[e^{(\varepsilon-\mu_n)/T} + 1]} \quad (B21)$$

and

$$\lambda_{\max}(\varepsilon) := \frac{1}{\hbar} \sqrt{2mR_0^2(\varepsilon + V_0)}. \quad (B22)$$

We wish to compare the result (B21) with the partial width $\Gamma_{\nu}^{\alpha\beta}(E^*, \Lambda)$ for the decay of a nucleus of excitation energy E^* and vanishing total angular momentum ($\Lambda = 0$) by emission of a neutron of energy ε_{α} and orbital angular momentum λ_{β} as it is obtained from Weisskopf's theory (Refs. [15], [23])

$$\Gamma_n^{\alpha\beta} = \frac{2(2\lambda_{\beta} + 1)}{h \rho(E^*, \Lambda = 0)} \cdot \rho_R(E_R^*, \Lambda_R) w_n(\varepsilon_{\alpha}, \lambda_{\beta}). \quad (B23)$$

In (B23), $\rho(E^*, \Lambda)$ and $\rho_R(E_R^*, \Lambda_R)$ are the level densities for the mother and daughter nucleus, resp., which depend on the excitation energy $E^*(E_R^*)$ and the total angular momentum $\Lambda(\Lambda_R)$

of the mother (daughter) nucleus. The quantity $w_n(\varepsilon_\alpha, \lambda_\beta)$ is the transmission factor for a neutron having the energy ε_α and the orbital angular momentum λ_β . The factor $2(2\lambda_\beta + 1)$, represents the product of the degeneracy factors of the emitted neutron and of the residual daughter nucleus. We note that, in the derivation of Eq. (B23) and also in our model, effects of the spin-orbit coupling on the emission probability are neglected. We now use the level densities obtained in the Fermi gas model:

$$\rho_R(E_R^*, 0) = \left(\frac{\hbar^2}{2J}\right)^{3/2} \sqrt{a} \frac{\exp(2\sqrt{aE_R^*})}{12E_R^{*2}}, \quad (B24)$$

$$\rho(E^*, 0) = \left(\frac{\hbar^2}{2J}\right)^{3/2} \sqrt{a} \frac{\exp(2\sqrt{aE^*})}{12E^{*2}}. \quad (B25)$$

Here J is the rigid body moment of inertia of the nucleus which is assumed to be the same for the mother and daughter nucleus, and "a" is the level density parameter.

The excitation energies E^* and E_R^* are related by the energy conservation

$$E^* = E_R^* + \varepsilon_\alpha - \mu_n. \quad (B26)$$

The ratio of the level densities is thus given by

$$\frac{\rho_R}{\rho} = \left(\exp\left[2\sqrt{aE_R^*} - 2\sqrt{aE^*}\right]\right) \cdot \left(\frac{E^*}{E_R^*}\right)^2 \quad (B27)$$

$$\frac{\rho_R}{\rho} = \left(\exp\left[2\sqrt{aE^*} \cdot \left(\sqrt{1 - \frac{\varepsilon_\alpha - \mu_n}{E^*}} - 1\right)\right]\right) \cdot \left(1 - \frac{\varepsilon_\alpha - \mu_n}{E^*}\right)^{-2}.$$

Assuming that the ratio $(\varepsilon_\alpha - \mu_n)/E^*$ is much smaller than 1

$$\frac{\varepsilon_\alpha - \mu_n}{E^*} \ll 1 \quad (B28)$$

and using the relation between the excitation energy E^* and the temperature T as given by the Fermi gas model

$$E^* = aT^2 \quad (B29)$$

we obtain for the ratio of the level densities

$$\frac{\rho(E_R^*)}{\rho(E^*)} \approx \exp\left(-\frac{\varepsilon_\alpha - \mu_n}{T}\right). \quad (B30)$$

Using (B30) we obtain for the neutron width (B23)

$$\Gamma_n^{\alpha\beta} \approx \frac{2(2\lambda_\beta + 1)}{h} e^{-\frac{\varepsilon_\alpha - \mu_n}{T}} \cdot w_n(\varepsilon_\alpha, \lambda_\beta). \quad (B31)$$

This form of Weisskopf's general formula agrees indeed with our result (B21) if the transmission factor w_n is calculated classically ($w_n = w_0^d$), if the orbital angular momentum λ_β is large enough so that

$$2\lambda_\beta + 1 \approx 2\lambda_\beta \quad (B32)$$

and if

$$\exp\left(\frac{\varepsilon_\alpha - \mu_n}{T}\right) \gg 1, \quad (B33)$$

so that the Fermi occupation factor in (B21) becomes equivalent to the Boltzmann factor

$$\frac{1}{e^{\frac{\varepsilon_\alpha - \mu_n}{T}} + 1} \approx e^{-\frac{\varepsilon_\alpha - \mu_n}{T}}. \quad (B34)$$

We note that the approximation (B34) is already used for obtaining the level density formula (B25) from the Fermi-gas model.

We would like to comment that the well-known formula (B23) is already a slight extension of the original result of Weisskopf published in Ref. [22]. There, the transmission factor w_n is expressed in terms of the cross-section for the absorption of a neutron by the daughter nucleus using detailed balance. In this form, Weisskopf's result is of very general validity. The difficulty with it is only that detailed balance relates the transmission factor w_n to the cross-section for absorption of a neutron by a nucleus with excitation energy E_R^* and angular momentum Λ_R . This absorption cross-section can, of course, not be measured. Therefore, one needs a model to calculate the transmission factor.

The considerations in this appendix demonstrate at the same time that it is meaningful to replace the purely classical transmission factor w_0^{cl}

$$w_0^{cl}(\varepsilon, l) = \theta_0 \left(\varepsilon + V_0 - \frac{l^2}{2MR_0^2} \right) \quad (B35)$$

by a quantum-mechanical barrier penetration factor as it is done in all our numerical calculations.

Table captions:

1. Multiplicities of the prefission particles emitted by: ^{126}Ba ^{188}Pt and $^{266,272,278}110$ at different excitation energies. The theoretical estimates for the compound nuclei with $Z=110$ are done for two values of the friction force. In the first rows are the data evaluated with the friction reduced by 50% while those in the second row correspond to the standard wall-and-window friction.

Figure captions:

1. The differential fusion (solid lines) and fission (bars) cross sections for the compound nucleus ^{126}Ba for different entrance channel reactions.
2. The deformation potential V_{fiss} for ^{126}Ba as a function of the "fission variable" R_{12}/R_0 from the ground state deformation up to the scission point. The different curves correspond to the different values of the angular momentum L . The temperature of ^{126}Ba is fixed at $T=1.6$ MeV.
3. The same as in Fig. 2, but now the different curves correspond to the different temperatures T . All plots are done for $L=30\hbar$. The different curves are shifted vertically in order to make the relative changes more visible.
4. The temperature of the compound nucleus ^{126}Ba at the different excitation energies as a function of angular momentum.
5. The multiplicities of prefission particles as a function of excitation energy of the compound nucleus ^{126}Ba obtained with the entrance channel $^{28}\text{Si} + ^{98}\text{Mo}$.
6. The same as in Fig. 5 but for the reaction $^{19}\text{F} + ^{107}\text{Ag}$.
7. The same as in Fig. 1 but for the compound nucleus ^{188}Pt .
8. The same as in Fig. 2 but for the compound nucleus ^{188}Pt .
9. The same as in Fig. 3 but for the compound nucleus ^{188}Pt .
10. The same as in Fig. 1 but for the compound nucleus $^{272}110$.
11. The same as in Fig. 2 but for the compound nucleus $^{266}110$ and temperature $T=0$.
12. The experimental (points with error bars) and theoretical multiplicities of prefission neutrons as a function of the excitation energy of the compound nuclei with $Z=110$ obtained in four different reactions.

Table 1

CN	Reaction	E_{lab}	E^*	M_n^{exp}	δM_n^{exp}	M_n	M_p	M_α
		MeV	MeV	-	-	-	-	-
^{126}Ba	$^{28}\text{Si} + ^{98}\text{Mo}$	204.0	131.7	2.52	0.12	2.29	0.03	0.79
		187.2	118.5	2.01	0.13	1.71	0.00	0.09
		165.8	101.4	1.32	0.09	1.83	0.00	0.04
		142.8	84.1	-	-	0.27	0.04	0.88
	$^{19}\text{F} + ^{107}\text{Ag}$	147.8	118.5	1.85	0.11	1.99	0.00	0.16
128.0		101.5	1.31	0.17	1.80	0.01	0.06	
^{188}Pt	$^{34}\text{S} + ^{154}\text{Sm}$	202.6	100.0	4.5	0.7	3.52	0.00	0.10
		159.8	66.5	2.5	0.7	1.10	0.00	0.00
	$^{16}\text{O} + ^{172}\text{Yb}$	137.6	99.7	5.4	0.6	3.79	0.00	0.06
$^{266}_{110}$	$^{58}\text{Ni} + ^{208}\text{Pb}$	513.9	185.9	7.83	0.46	8.66	0.26	1.04
						9.72	0.23	0.95
		486.6	164.6	7.35	0.50	7.65	0.20	0.93
						8.56	0.21	0.79
		461.1	144.6	6.17	0.48	6.50	0.16	0.81
						7.30	0.17	0.73
		436.2	125.1	4.74	0.49	5.45	0.10	0.63
						6.21	0.11	0.58
		410.1	104.7	4.41	0.41	4.35	0.07	0.48
						4.94	0.07	0.48
		377.0	78.8	2.94	0.36	2.77	0.03	0.30
				3.23	0.03	0.33		
$^{272}_{110}$	$^{64}\text{Ni} + ^{208}\text{Pb}$	472.3	138.3	5.98	0.43	7.49	0.08	0.42
						8.25	0.08	0.34
		449.9	121.1	5.52	0.38	6.40	0.05	0.30
						7.12	0.06	0.28
		423.0	100.6	5.13	0.33	5.09	0.02	0.20
						5.58	0.04	0.20
		403.9	85.9	3.54	0.31	3.94	0.01	0.15
						4.49	0.01	0.12
	$^{40}\text{Ca} + ^{232}\text{Th}$	377.0	65.3	3.03	0.32	2.27	0.00	0.10
						2.83	0.00	0.08
		351.2	166.3	8.40	0.53	9.23	0.13	0.53
						9.95	0.15	0.48
		298.4	121.3	5.81	0.50	6.40	0.05	0.30
						7.12	0.06	0.28
$^{278}_{110}$	$^{40}\text{Ar} + ^{238}\text{U}$	250.4	80.3	3.35	0.34	3.56	0.01	0.14
						4.04	0.01	0.12
		299.6	127.2	5.78	0.51	7.89	0.03	0.14
						8.48	0.04	0.15
		280.4	110.7	4.96	0.55	6.69	0.00	0.12
						7.23	0.03	0.13
		258.0	91.5	4.22	0.44	5.08	0.00	0.09
				5.59	0.00	0.09		

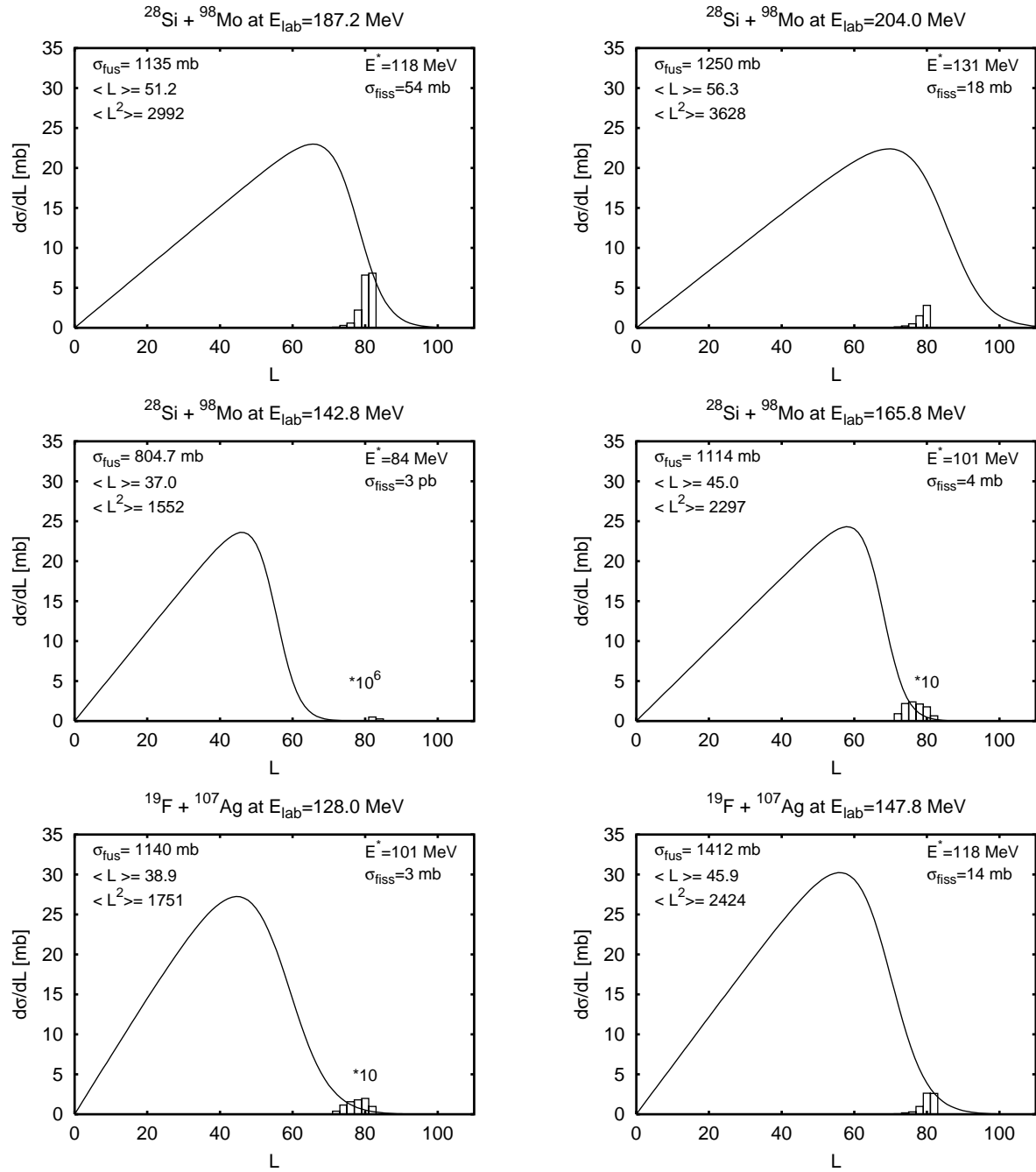


Figure 1:

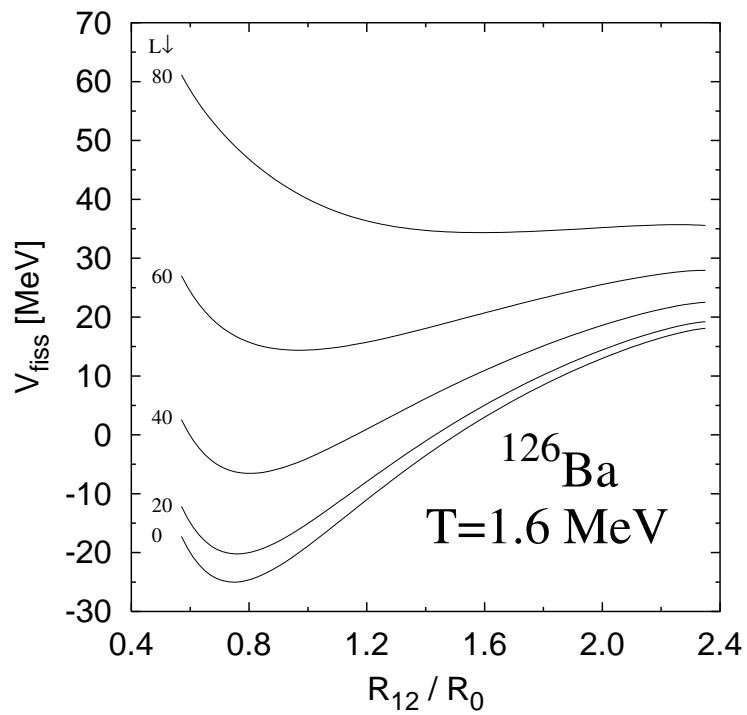


Figure 2:

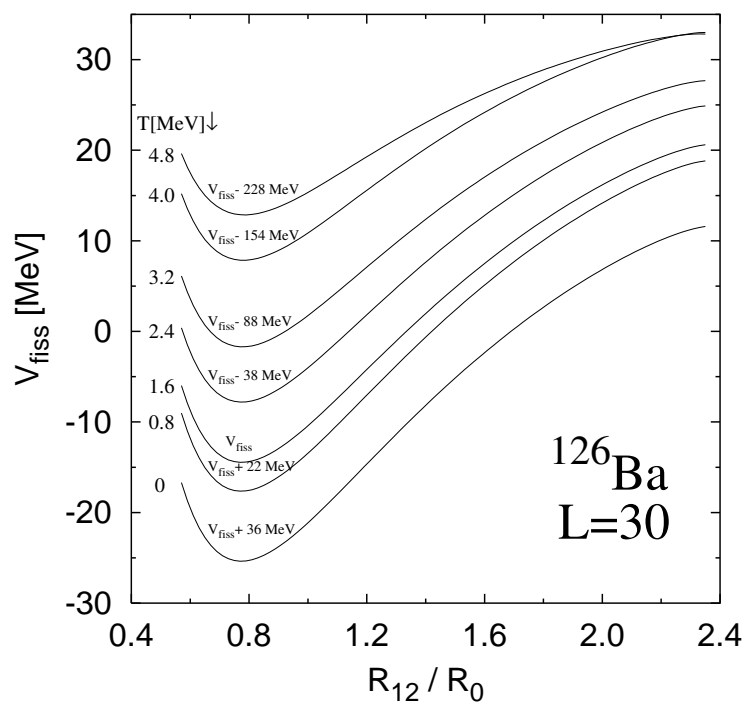


Figure 3:

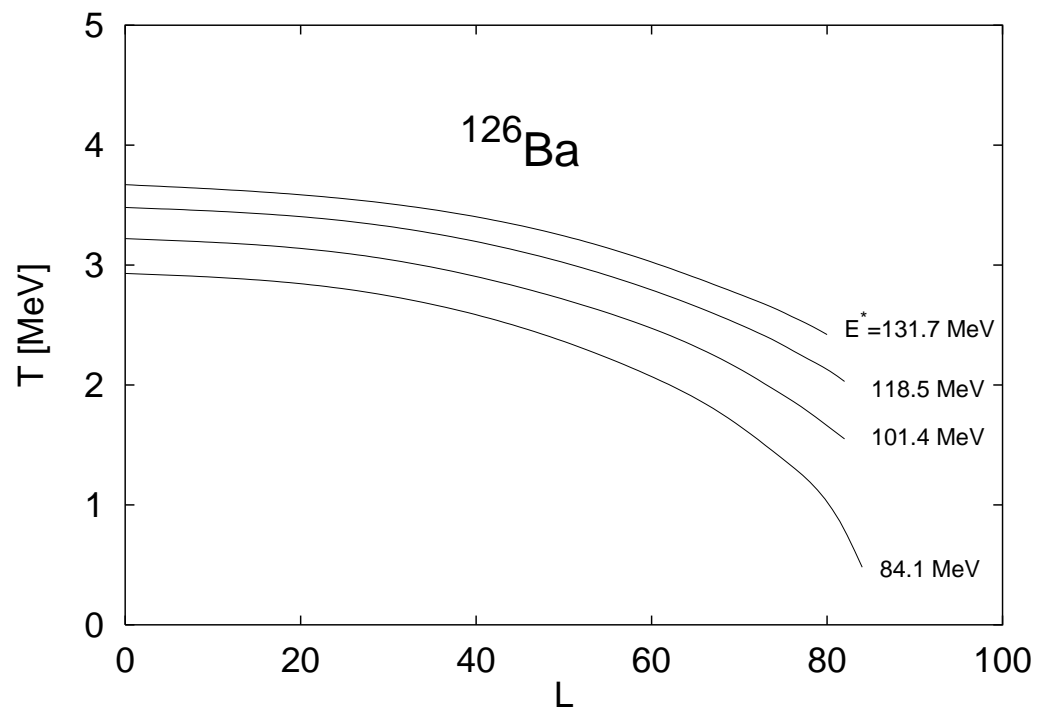


Figure 4:

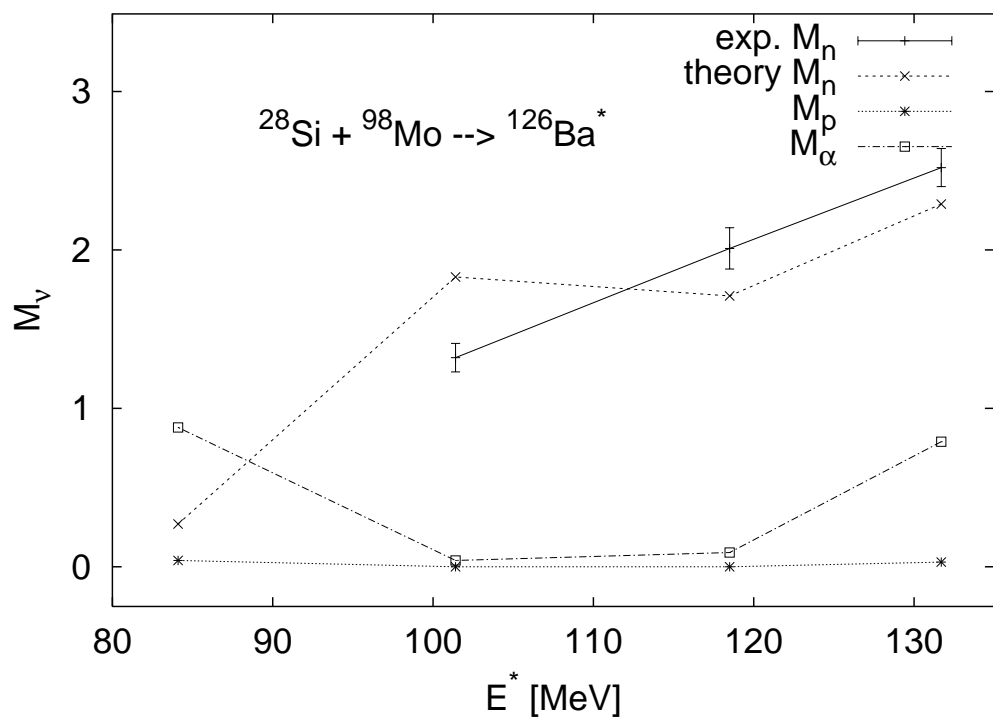


Figure 5:

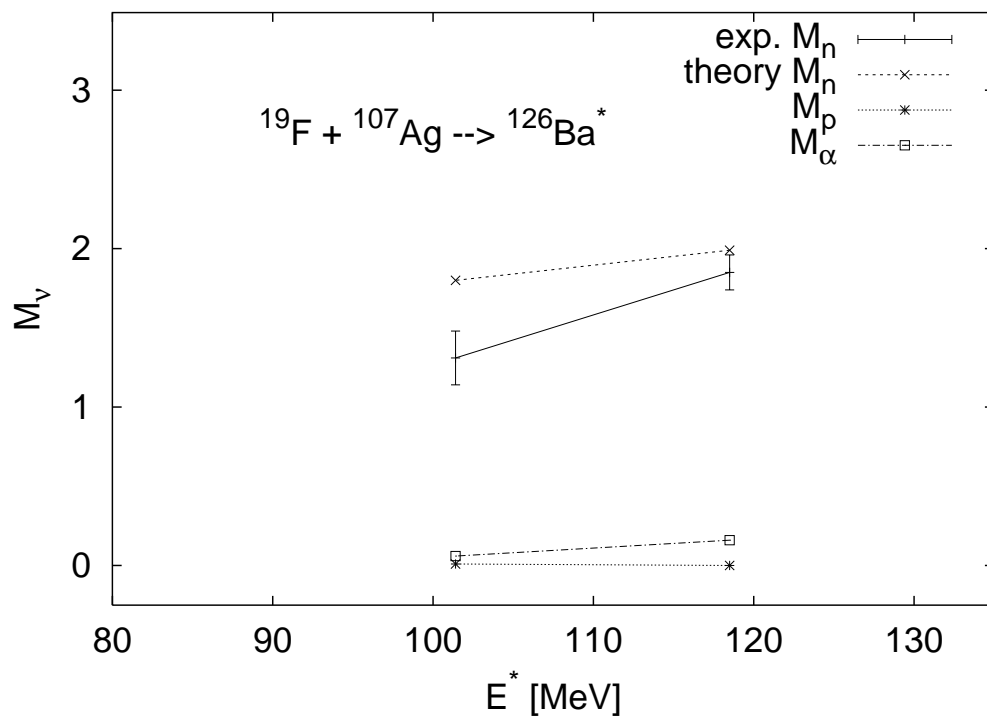


Figure 6:

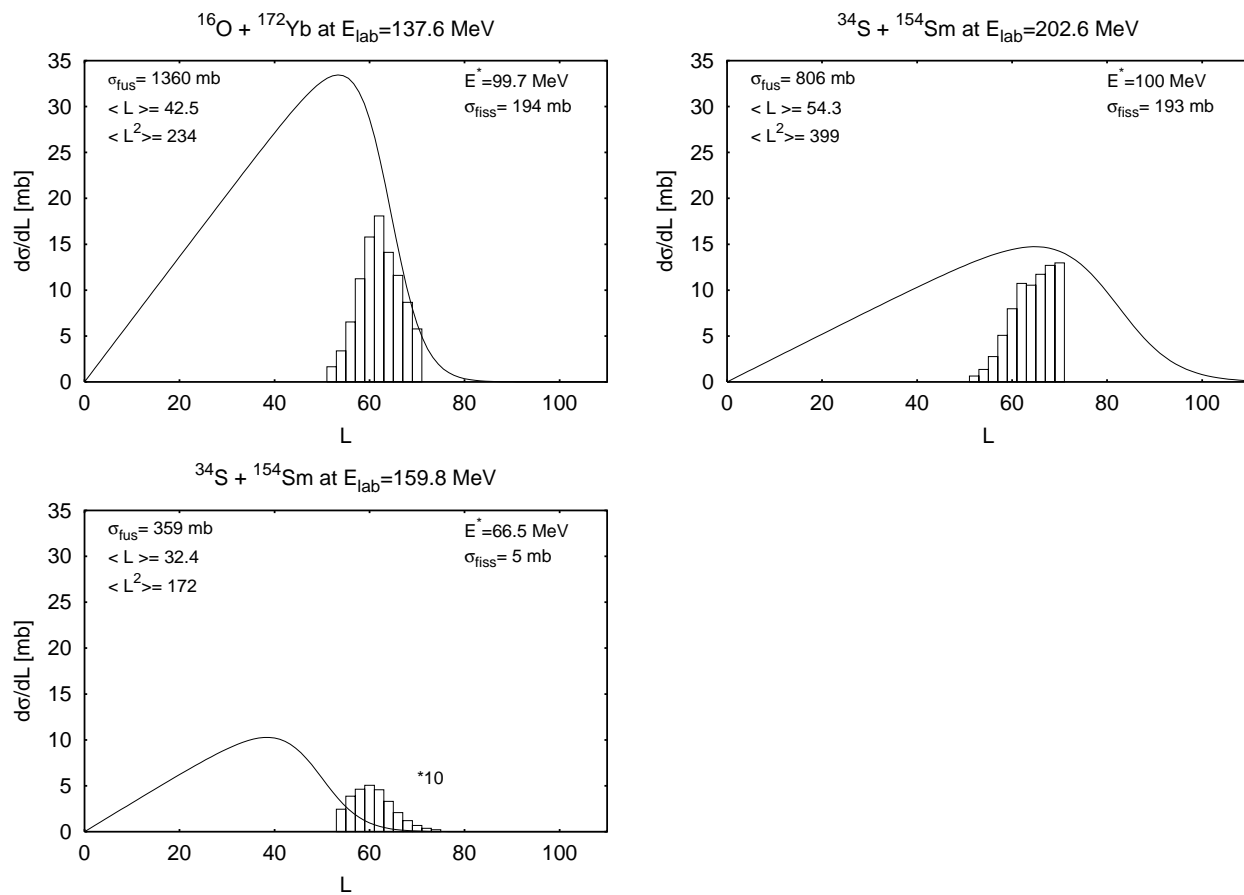


Figure 7:

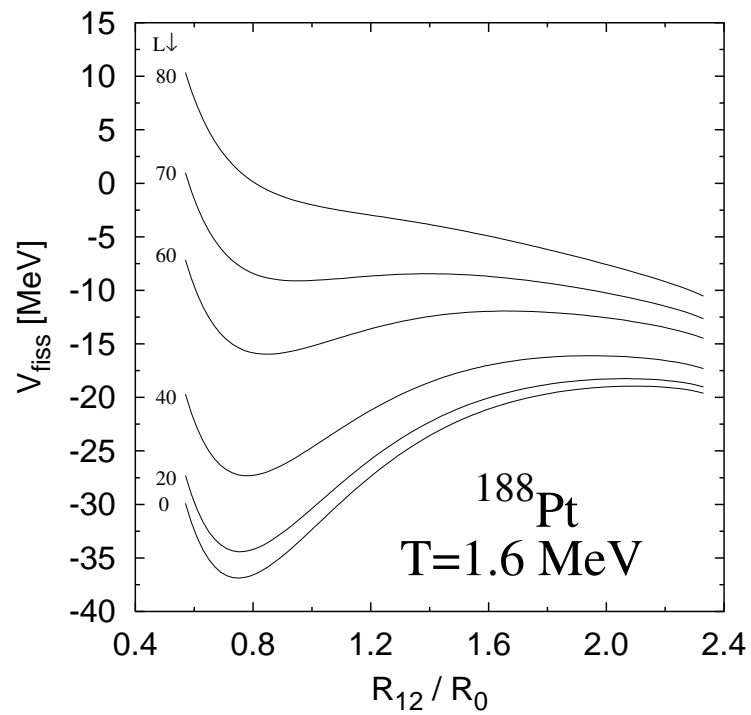


Figure 8:

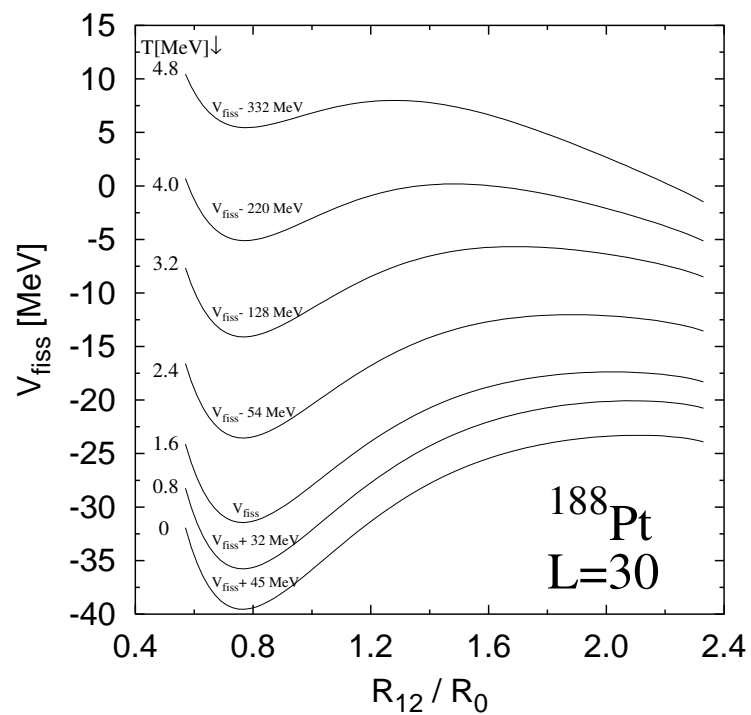


Figure 9:

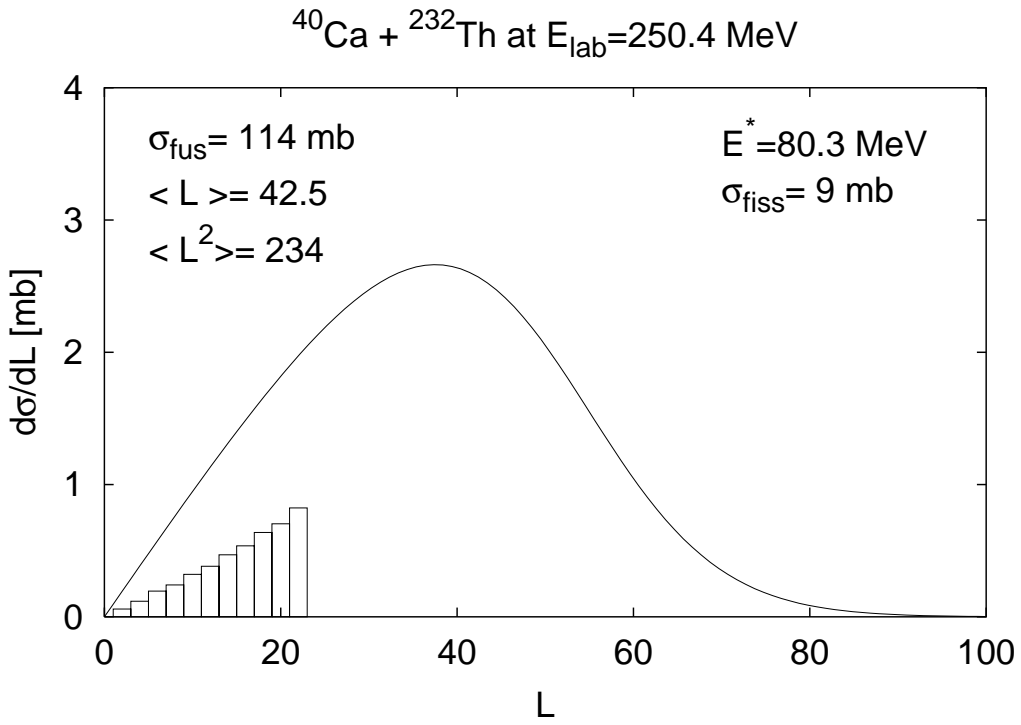


Figure 10:

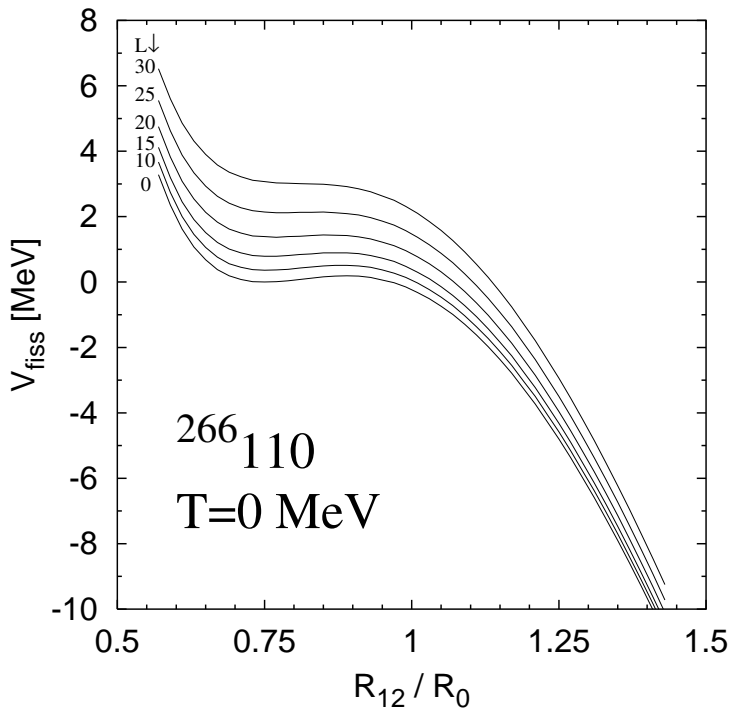


Figure 11:

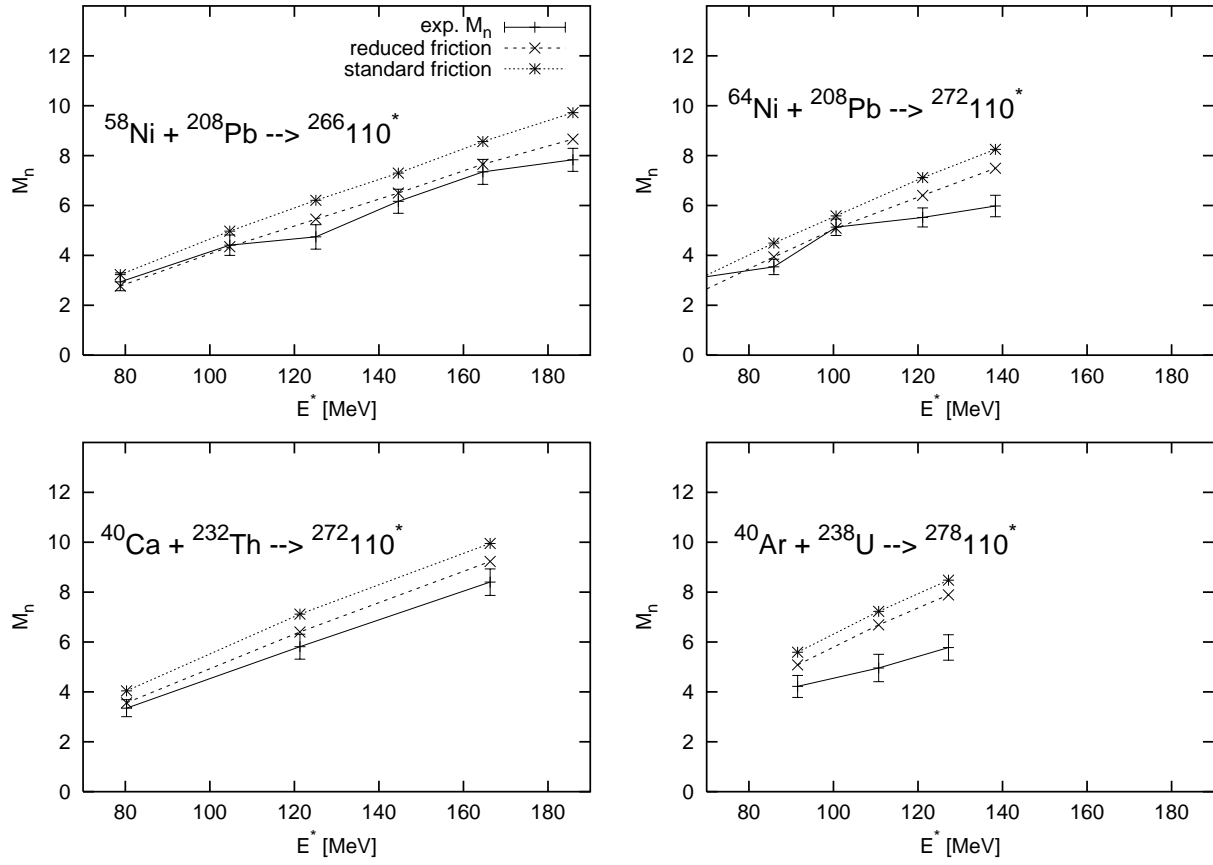


Figure 12: